Supporting Information

Defect passivation by alcohol-soluble small molecule for efficient *p-i-n* planar perovskite solar cells with high open-circuit voltage

Kang Chen[§ a], Jingnan Wu [§ a], Yanan Wang* [a], Qing Guo [a], Qiaoyun Chen [a], Tiantian Cao [a], Xia Guo [a], Yi Zhou [a], Ning Chen* [a], Maojie Zhang* [a], Yongfang Li [a, b]

[a] *Laboratory of Advanced Optoelectronic Materials, College of Chemistry, Chemical Engineering and Materials Science, Soochow University, Suzhou 215123, China.*

E-mail: yananw@suda.edu.cn; chenning@suda.edu.cn; mjzhang@suda.edu.cn;

[b] *Beijing National Laboratory for Molecular Sciences, Institute of Chemistry, Chinese Academy of Sciences, Beijing, 100190, PR China*

[§]*These authors contributed equally to this work.*

Materials

Fullerene C_{60} (99.9%) was purchased from Dade Carbon Nanotechnology Co., Ltd, Methylammonium iodide (MAI) was synthesized in our laboratory according to the literature.[1] PbI_2 (99.999%) was bought from Alfa Aesar, Methylammonium Chloride (MACl), poly(bis(4-phenyl)(2,4,6-trimethylphenyl)amine)(PTAA) (Mn=6000-15000) and 2,9-dimethy-4,7-diphenyl-1,10-phenanthtoline (BCP) (99%) was purchased from Xi'an Polymer Light Technology Crop.

Device fabrication.

ITO glass was cleaned by ultrasonic bath of detergent, deionized water, acetone, ethanol, and isopropyl alcohol for 15 min, respectively. Before using, the ITO glass was dried with N_2 and heated for 5 min on a 100^{o}C heat plate. 2 mg PTAA was dissolved in toluene and stirred for 12 h. 30 uL toluene solution was spin-coated on ITO substrates at 5000 rpm for 30 s in glove box with nitrogen atmosphere. Then the substrates were annealed at 100^{o}C for 10 min.

461mg PbI_2 was dissolved in 1 mL mix solvent of N, N-dimethylformamide (DMF) and dimethyl sulfoxide (V:V=95:5), and stirred at 70^{o}C for 12 h. 50 mg MAI ,5mg MACl and 2,5-di(thiophen-2-yl)terephthalic acid (DTA) with different doping doses (0, 0.25, 0.5, 1, 2, and 3 mg) were dissolved in 1mL isopropanol (IPA) and stirred at room temperature for 12 h. Before used, all these precursor solutions were filtered by 0.45 um polytetrafluoroethylene (0.45 um) filter. Sequential two-step deposition method was used to deposite the perovskite layer. Simply, 40 uL PbI_2 solutions was spun onto PTAA at 4500 rpm for 45s. During this period, 40 uL IPA mix solution was cast on spinning substrates in the 20 s, and then, annealed at 95^{o}C for 3 min.

The substrates with perovskite active layer were transferred into vacuum evaporation warehouse to thermally evaporate 20 nm C_{60} and 7 nm BCP. Finally, 80 nm Ag was vacuum evaporate as a counter electrode. A shadow mask with an area of 0.0757 cm^2 was used to fix measuring area.

Martials and devices characterization

The instrument of Bruker VERTEX 70 V (Germany) was used to test Fourier transform infrared spectrometer (FTIR) spectra. Thermal gravimetric analysis (TGA) was obtained with a PerkinElmer Pyris 6. Current density−voltage (*J*−*V*) curves of perovskite solar cells (Pero-SCs) were acquired by applying an external voltage bias and using Keithley 2400 digital source meter

to record the current response. A Xenon arc lamp with power of 100 mW/cm^2 simulated Air Mass 1.5 global (AM 1.5G) solar illumination. Steady-state photocurrents under applied voltage were obtained in the same instrument. The measurements of *J-V* and steady-state photocurrents were carried out in glove box. External quantum efficiency (EQE) of (Pero-SCs) was measured using Enli Technology Co., Ltd. QE-R3011 in air without bias light. Standard commercial single-crystal silicon solar cells were used to corrected illumination intensities. SU8010 (Hitachi produced) was used to acquire scanning electron microscopy (SEM) images. X-ray photoelectron spectroscopic (XPS) was measured by Escalab 250Xi (Thermo Fisher, USA). X-ray diffraction (XRD) patterns (2θ scans) were recorded by X-ray diffractometer (D2 PHASER, Bruker, Germany) from 10 to 60 with radiation source angle λ=1.54184 Å. Ultraviolet-visible (UV-vis) spectra was carried out using an UV-vis spectrophotometer (Cary 6000, Agilent). Steady-state photo-luminescence (PL) was measured on FLS980 (Edinburgh Instrument, UK) with excitation wavelength is 470 nm. Time-resolved PL spectra was acquired on Lifespec (Edinburgh Instrument, UK) with a 477 nm laser (5 MHz).

Characterizations

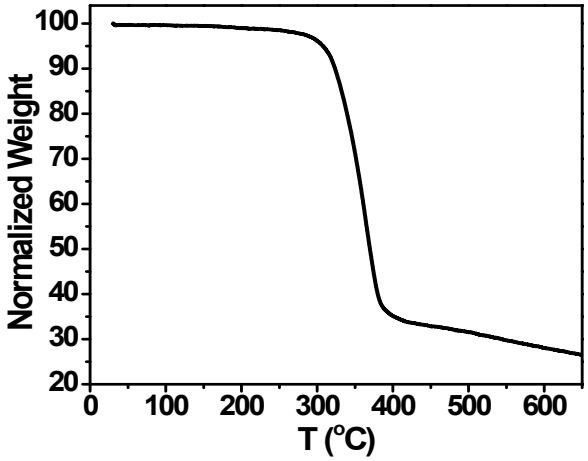

Fig. S1. TGA plot curve of DTA with a heating rate of 10 °C/min under nitrogen atmosphere.

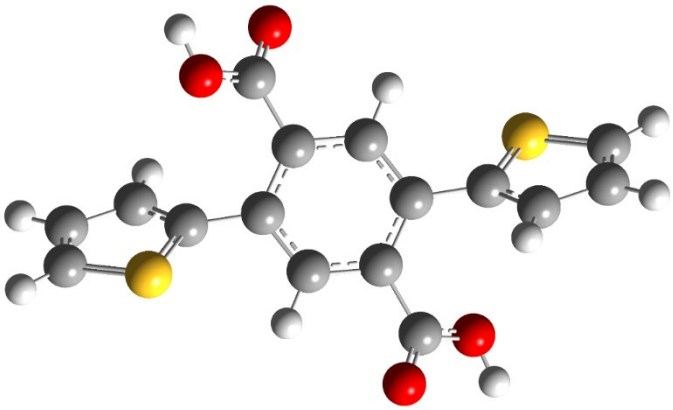

Fig. S2. Optimal geometries of DTA calculated at B3LYP/6-31G** level

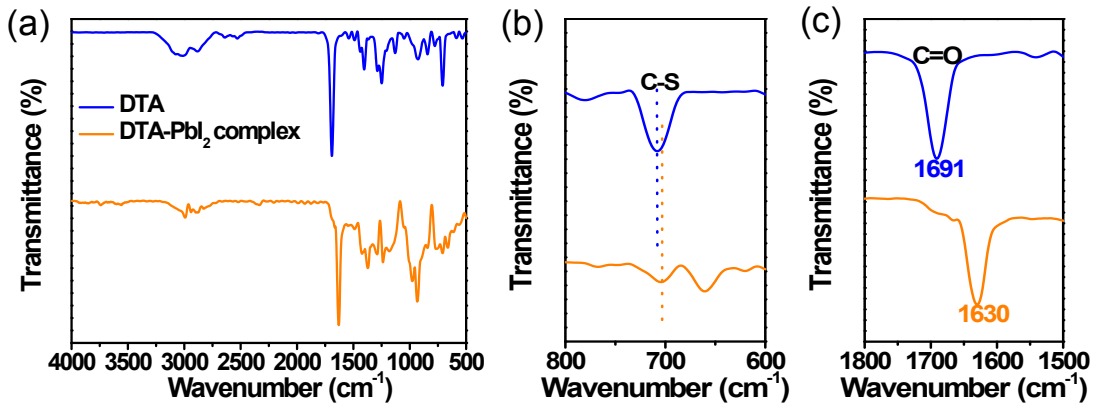

Fig. S3. (a) FTIR spectra of pure DTA and DTA-PbI_2 complex. (b) Magnification spectra of C-S vibration from the part wavelength of (a). (c) Magnification spectra of C=O vibration from the part wavelength of (a). (DTA-PbI_2 complex: PbI_2 and DTA with the molar ratio 1:1 were dissolved in DMF and stirred for one night at room temperature, and then the DMF was removed to obtain the DTA-PbI_2 complex.)

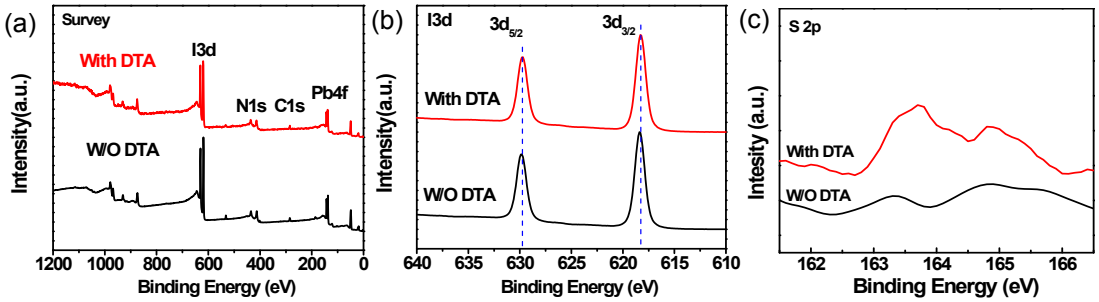

Fig. S4. (a) XPS survey spectrum of $MAPbI_{3-x}Cl_x$ film without and with DTA. High-resolution XPS of I 3d (b) and S 2p (c) from $MAPbI_{3-x}Cl_x$ film without and with DTA.

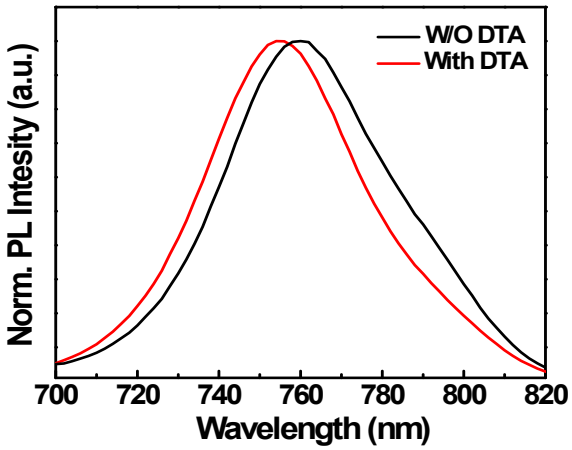

Fig. S5. Normalized steady-state PL spectra of the $MAPbI_{3-x}Cl_x$ films without and with DTA passivation.

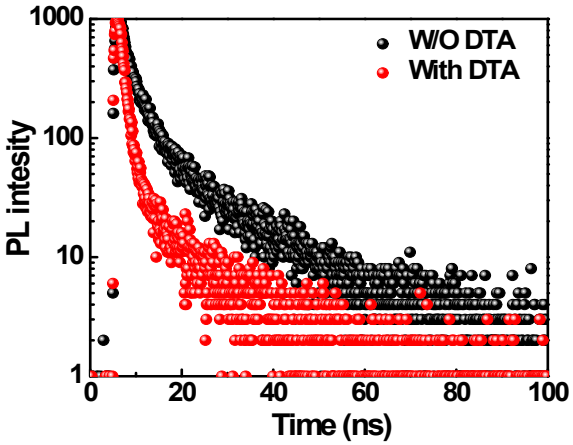

Fig. S6. Time-resolved PL spectra of the $MAPbI_{3-x}Cl_x$ films with coated-PCBM films without and with DTA passivation deposited on bare glass substrate.

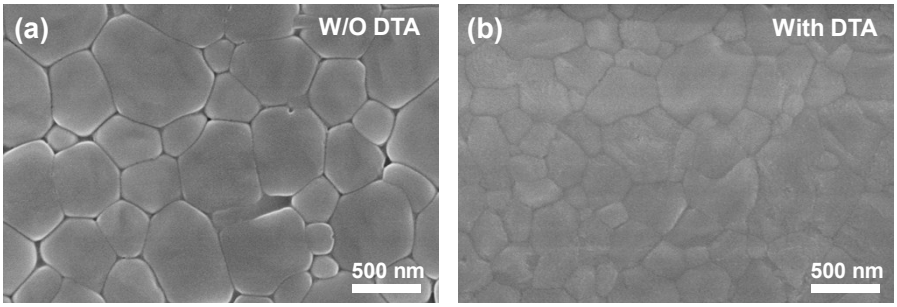

Fig. S7. Top-view SEM images of $MAPbI_{3-x}Cl_x$ films (a) without and (b) with DTA deposited on bare glass.

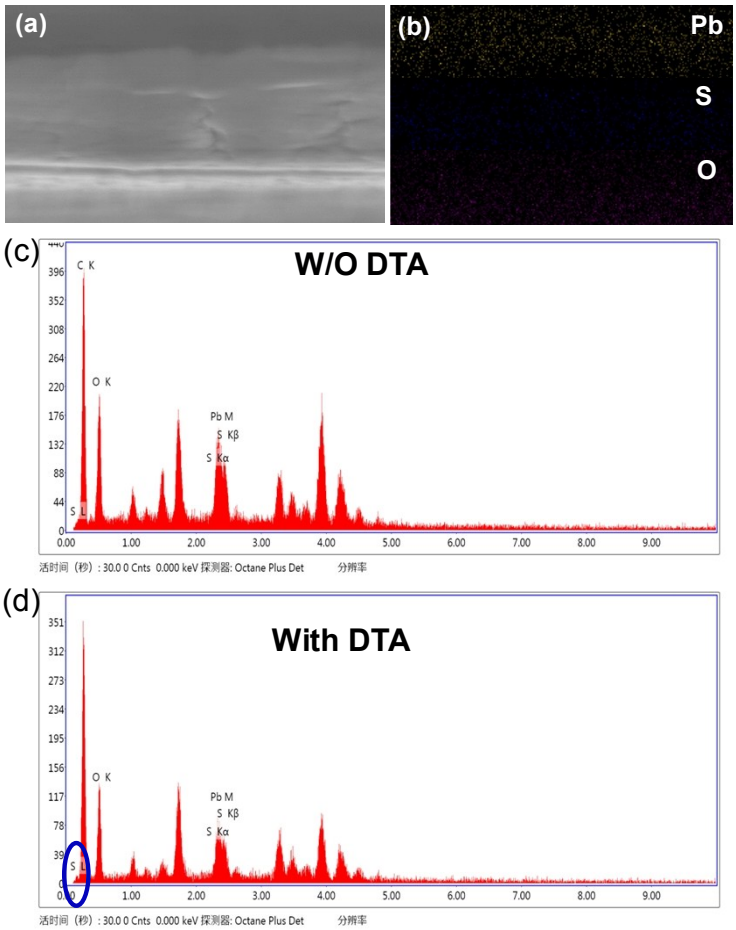

Fig. S8. (a) Cross-sectional SEM of $MAPbI_{3-x}Cl_x$ film without DTA deposited on the PTAA-coated ITO. (b) The corresponding elemental maps of $MAPbI_{3-x}Cl_x$ film without DTA. The EDS spectrum of $MAPbI_{3-x}Cl_x$ film without DTA (c) and with DTA (d).

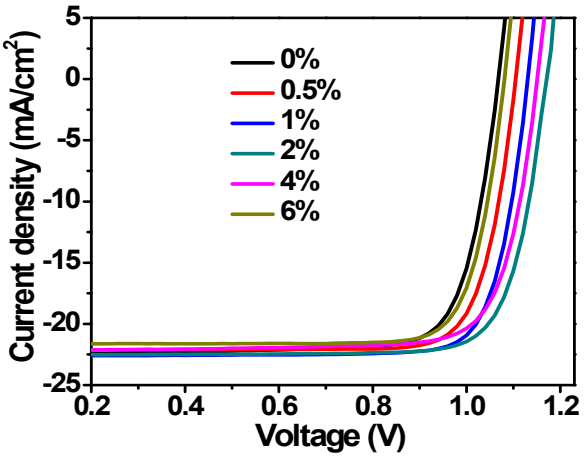

Fig. S9. *J-V* characteristics for devices with different mass ratios of DTA additive.

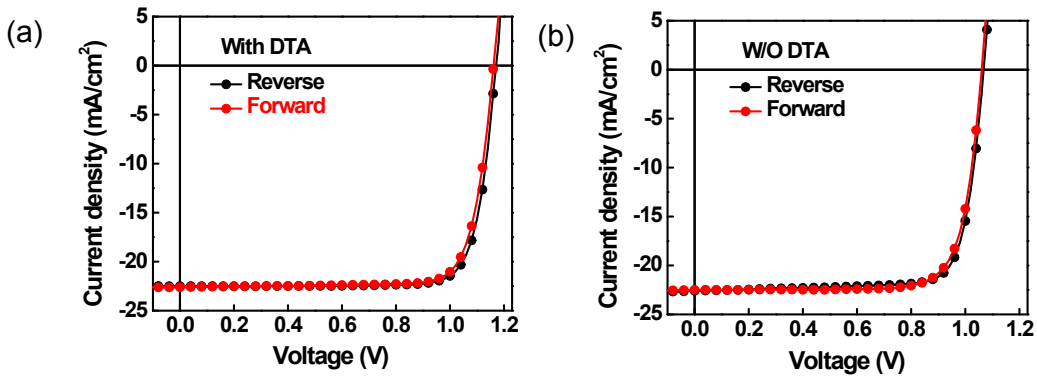

Fig. S10. *J-V* curves of the champion devices obtained from reverse scan and forward scan without (a) and with DTA passivation (b).

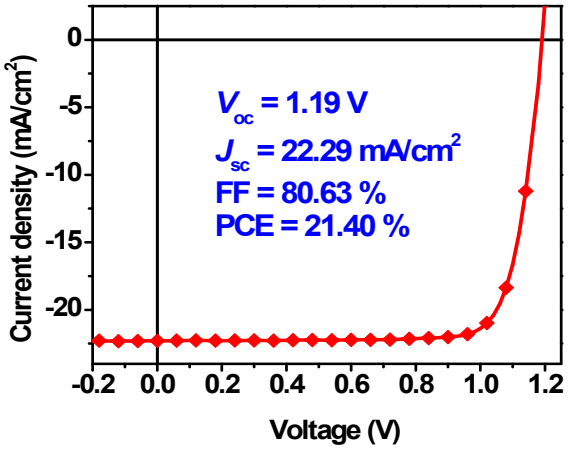

Fig. S11. *J-V* curve of device with the highest $V_{oc.}$

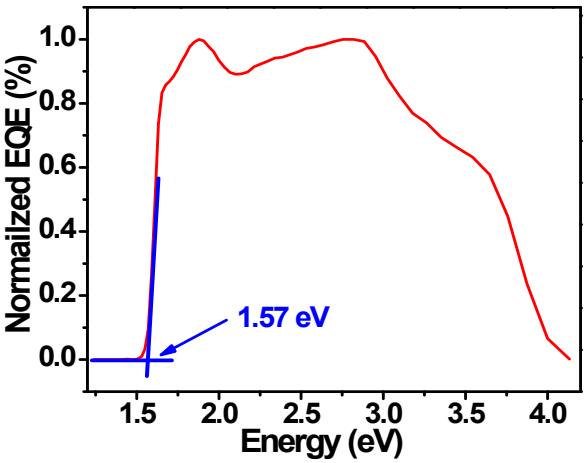

Fig. S12. EQE spectra of a $MAPbI_{3-x}Cl_x$ Pero-SCs revealing the onset at ~ 1.57 eV. (The x axis is calculated from 1240/wavelength of EQE)

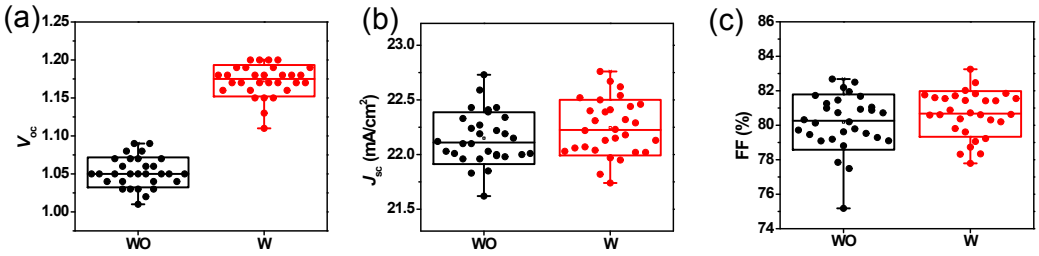

Fig. S13. V_{oc}, J_{sc} and FF distributions in a box chart based on 30 devices without and with 2% DTA passivated.

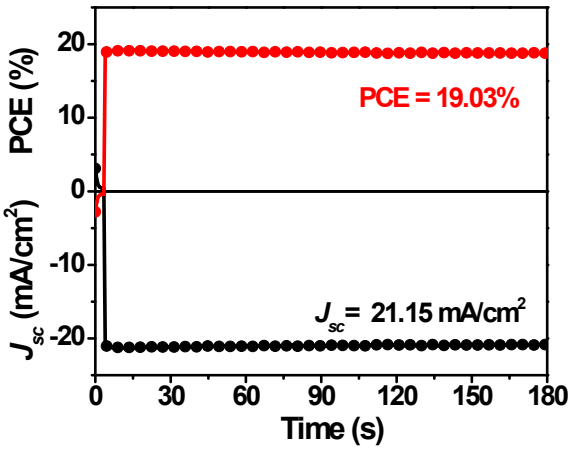

Fig. S14 Steady-state photocurrent and efficiency for the best control device.

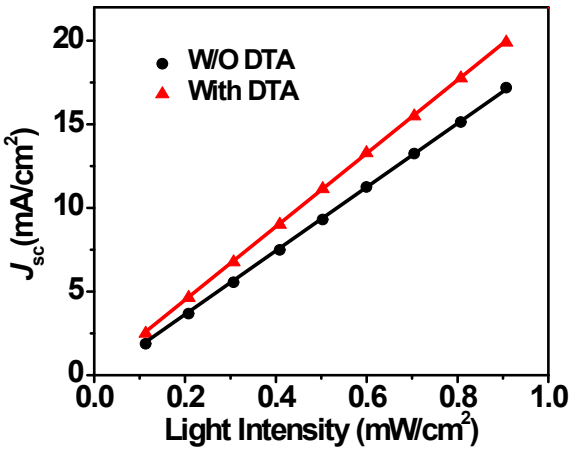

Fig. S15. Light intensity dependence of J_{sc} for control and passivated devices.

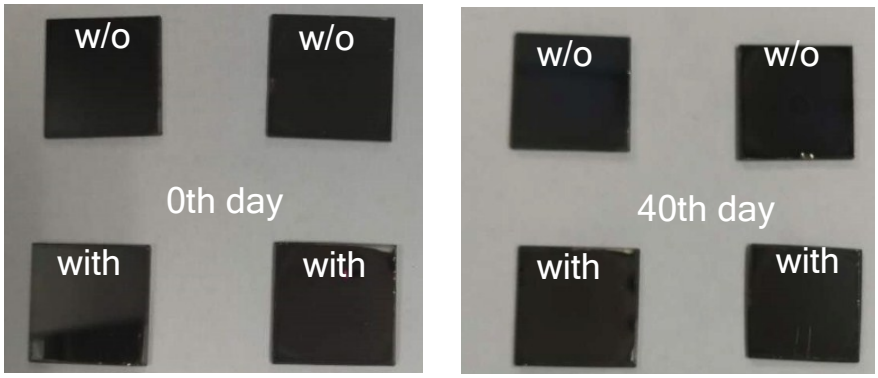

Fig. S16. Photographs of the $MAPbI_{3-x}Cl_x$ films without and with DTA passivation before and after humidity aging for 40 days.

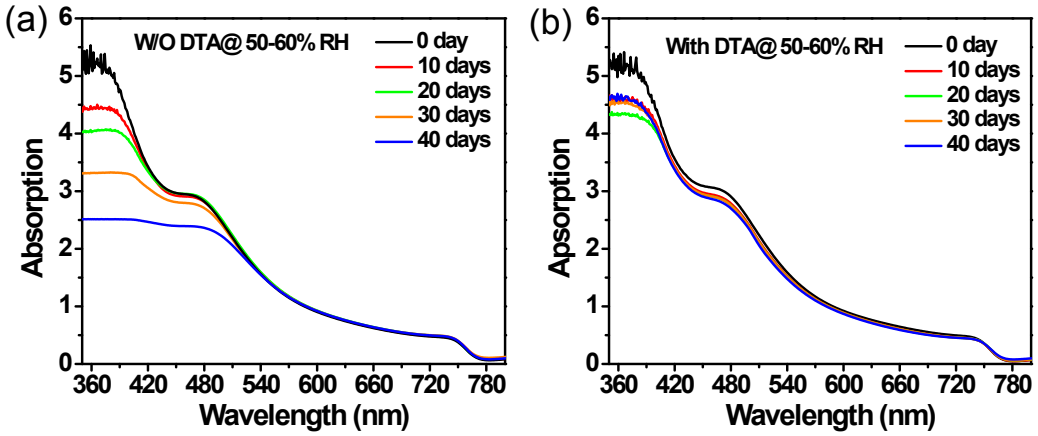

Fig. S17. Monitoring degradation of perovskite films without (a) and with DTA passivation (b) under a relative humidity of 50-60% by UV-vis absorption spectroscopy.

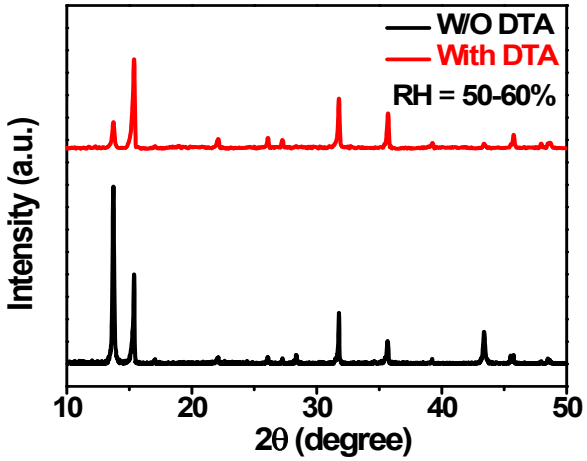

Fig. S18. The XRD patterns of perovskite films without and with DTA passivation stored in ambient air with a relative humidity 50%-60% for 40 days.

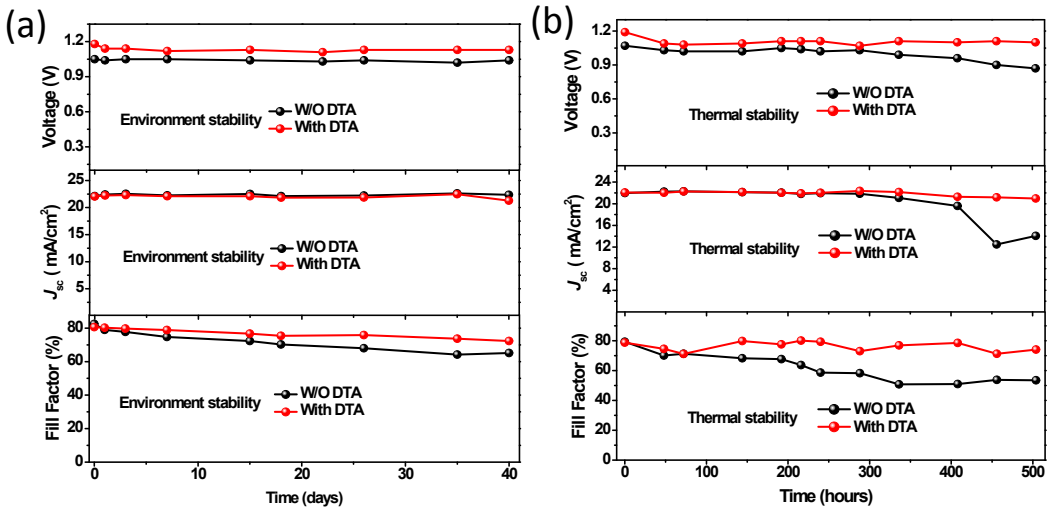

Fig. S19. (a) The corresponding photovoltaic parameters changes of unsealed Pero-SCs without and with DTA passivation exposed in ambient environment with a relative humidity 15%-20% in the dark at 20-25^{o}C over time. (b) The corresponding photovoltaic parameters changes of Pero-SCs without and with DTA passivation holed at 65^{o}C in glovebox over time.

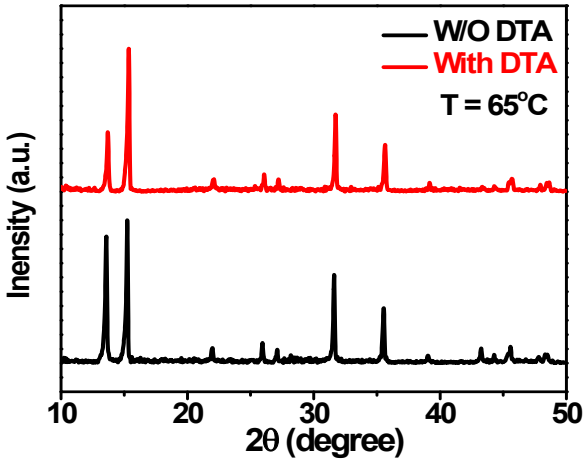

Fig. S20. The XRD patterns of perovskite films without and with passivation holed at 65°C for 10 days.

Table. S1 The fitting parameters of time-resolved PL decays for the corresponding samples.

	A_1 (%)	τ_1 (ns)	A_2 (%)	τ_2 (ns)
W/O	30.6	2.2	69.4	19.4
With	24.2	29.9	75.8	194.3

Table. S2 Photovoltaic performance of devices with different mass ratios of DTA in organic salts precursor solutions.

Mass ratio	V_{oc} (V)	J_{sc} (mA/cm^2)	FF (%)	PCE (%)
0	1.05±0.02	22.17±0.24	80.44±1.30	18.71±0.31
0.5%	1.10±0.01	22.33±0.37	80.78±1.73	19.78±0.57
1%	1.13±0.01	22.24 ±0.23	81.67±1.02	20.42±0.29
2%	1.17±0.02	22.26±0.23	80.71±1.12	21.06±0.34
4%	1.15±0.02	22.10±0.28	79.70±1.84	20.22±0.47
6%	1.07±0.03	21.98±0.56	76.11±3.59	17.98±0.74

Table. S3 Summary of some top V_{oc} and PCE for *p-i-n* planar Pero-SCs in recent literatures.

Metal-halide perovskite	**V_{oc} (V)**	**J_{sc} (mA/cm^2)**	**FF (%)**	**PCE (%)**	**Literatures**
$MAPbI_3$	1.15	22.7	80.9	21.1	Ref.(2)
$MAPbI_3$	1.12	22.38	0.82	20.55	Ref.(3)
$MAPbI_3$	1.146	22.69	78.55	20.43	Ref.(4)
$MAPbI_3$	1.15	21.93	79.6	20.07	Ref.(5)
$MAPbI_3$	1.18	22.5	81.7	21.7	Ref.(6)
$MAPbI_{3-x}Cl_x$	1.14	21.36	78.9	19.16	Ref.(7)
$Cs_{0.05}FA_{0.81}MA_{0.14}PbI_{2.55}Br_{0.45}$	1.21	22.49	0.785	21.4(best)	Ref.(8)
	1.23(best)	22.16	0.775	21.12	
$FA_{0.85}MA_{0.15}Pb(I_{0.85}Br_{0.15})_3$	1.15	23.1	81.1	21.5	Ref.(2)
$(FA_{0.95}PbI_{2.95})_{0.85}(MAPbBr_3)_{0.15}$	1.21	22.50	0.790	21.51	Ref.(9)
$(MA_{0.17}FA_{0.83})Pb(I_{0.83}Br_{0.17})_3$	1.180	23.2	74.0	20.3	Ref.(10)
$MAPbI_{3-x}Cl_x$	1.17	22.50	81.42	21.45 (best)	This work
	1.19 (best)	22.29	80.63	21.40	

References

1. P. W. Liang, C. Y. Liao, C. C. Chueh, F. Zuo, S. T. Williams, X. K. Xin, J. Lin and A. K. Y. Jen, *Adv. Mater.*, 2014, **26**, 3748-3754.
2. Y. Bai, Y. Lin, L. Ren, X. Shi, E. Strounina, Y. Deng, Q. Wang, Y. Fang, X. Zheng, Y. Lin, Z. G. Chen, Y. Du, L. Wang and J. Huang, *ACS Energy Lett.*, 2019, DOI: 10.1021/acsenergylett.9b00608, 1231-1240.
3. D. Yang, X. Zhang, K. Wang, C. Wu, R. Yang, Y. Hou, Y. Jiang, S. Liu and S. Priya, *Nano Lett.*, 2019, **19**, 3313-3320.
4. T. Wu, Y. Wang, X. Li, Y. Wu, X. Meng, D. Cui, X. Yang and L. Han, *Adv. Energy Mater.*, 2019, **9**, 1803766.
5. W. Chen, Y. Zhou, G. Chen, Y. Wu, B. Tu, F. Z. Liu, L. Huang, A. M. C. Ng, A. B. Djurišić and Z. He, *Adv. Energy Mater.*, 2019, 1803872.
6. W. Q. Wu, Z. Yang, P. N. Rudd, Y. Shao, X. Dai, H. Wei, J. Zhao, Y. Fang, Q. Wang and Y. Liu, *Sci. Adv.*, 2019, **5**, ea8925.
7. Q. Chen, L. Yuan, R. Duan, P. Huang, J. Fu, H. Ma, X. Wang, Y. Zhou and B. Song, *Solar RRL*, 2019, **0**, 1900118.
8. S. Yang, J. Dai, Z. Yu, Y. Shao, Y. Zhou, X. Xiao, X. C. Zeng and J. Huang, *J. Am. Chem. Soc.*, 2019, **141**, 5781-5787.
9. D. Luo, W. Yang, Z. Wang, A. Sadhanala, Q. Hu, R. Su, R. Shivanna, G. F. Trindade, J. F. Watts, Z. Xu, T. Liu, K. Chen, F. Ye, P. Wu, L. Zhao, J. Wu, Y. Tu, Y. Zhang, X. Yang, W. Zhang, R. H. Friend, Q. Gong, H. J. Snaith and R. Zhu, *Science*, 2018, **360**, 1442-1446.
10. P. Caprioglio, F. Zu, C. M. Wolff, J. A. Márquez Prieto, M. Stolterfoht, P. Becker, N. Koch, T. Unold, B. Rech, S. Albrecht and D. Neher, *Sustainable Energy Fuels*, 2019, **3**, 550-563.